EFFECTIVENESS OF 1D GROUND RESPONSE ANALYSES AT PREDICTING SITE RESPONSE AT CALIFORNIA VERTICAL ARRAY SITES

Kioumars Afshari and Jonathan P. Stewart

Department of Civil & Environmental Engineering
University of California, Los Angeles

Abstract

We investigate the ability of 1-D ground response simulations to match observed levels of site amplification from California vertical arrays. Using 10 vertical arrays, we find simulations to best match data using a V_S-based damping model from the literature. We find a higher percentage of California sites, as compared to KiK-net sites from Japan, to have a reasonable match of empirical and theoretical transfer function shapes. The empirical transfer functions also have a greater degree of event-to-event consistency than has been found previously in Japan. Cases with poor matches highlight that 1-D simulations can fail to accurately model site response.

Introduction

Evaluating the role of local site conditions on ground shaking is an essential part of earthquake ground motion prediction, which can be done using ergodic models or site-specific analyses. One-dimensional (1D) simulation of shear waves propagating vertically through shallow soil layers, also known as ground response analysis (GRA), is a common approach for capturing the effects of site response on ground shaking. In GRA, different approaches have been used for modeling soil behavior, namely linear, equivalent-linear (EL), and various nonlinear (NL) methods. Much attention has been directed in recent research to which of these approaches is best suited to a particular problem, with the intention of guiding the selection of an appropriate method of analysis (e.g., choosing when NL is preferred to EL) (e.g., Kim et al., 2015; Kaklamanos et al, 2013, 2015; Zalachoris and Rathje, 2015). However, a crucial issue that has received much less attention is the degree to which 1D simulations (the essential assumption behind all GRA methods) are effective.

While site response can include important contributions from the wave propagation mechanics simulated in GRA, site response as a whole is considerably more complex. True site response represents the difference between ground motions for a given site condition and what would have occurred had the site had a reference condition (typically rock with a particular V_{S30}). Processes that can control site response in this context include surface waves, basin effects (including focusing and basin edge-generated surface waves), and topographic effects. Because GRA only simulates a portion of the physics controlling site response, there should be no surprise that it is not always effective at accurately predicting site effects.

Validation and testing of 1D GRA is possible by studying recordings from vertical array sites. The KiK-net array in Japan (Aoi et al., 2000) provides a large inventory of vertical arrays that has been extensively used for validation purposes (Thompson et al., 2012; Kaklamanos et al, 2013, 2015; Zalachoris and Rathje, 2015). As described in the next section, when viewed as a whole, these KiK-net data challenge the notion that 1D GRA provides a reliable estimate of site response. Were this result found to be widely applicable, it would upend a good deal of current practice that relies on GRA to estimate first-order site response. Our objective in this study, for which this paper provides preliminary results, is to utilize the growing body of vertical array data from California to investigate applicability of 1D GRA to predict observed site response. In short, we seek to answer the question – are the poor matches of 1D GRA from the KiK-net array a product of particular geological conditions at the sites in that array, and hence not generally applicable in California?

Prior Work Utilizing KiK-net Array Sites

Thompson et al. (2012) studied 100 KiK-net sites in Japan in order to assess the variability in site amplification and the performance of linear 1D GRA. These sites have recorded a large number of surface and downhole (in rock) recordings. The presence of multi-depth records enables the calculation of empirical transfer functions (ETFs) directly from surface $G(f,x_1)$ and downhole $G(f,x_2)$ amplitude spectra:

$$H(f) = \frac{G(f,x_1)}{G(f,x_2)} \tag{1}$$

where $H(f)$ is the ETF. For GRA, they used the program NRATTLE, which is a part of the ground motion simulation program SMSIM (Boore, 2005). NRATTLE performs linear GRA using quarter-wavelength theory. In order to minimize the potential for nonlinear effects, only records having a ground surface PGA < 0.1 g were selected.

ETFs were computed with Eq. (1) using available data meeting certain selection requirements. In total, 3714 records from 1573 earthquakes were considered for the 100 KiK-net sites. The mean and 95% confidence intervals were computed across all selected recordings at a given site, with the example results (for two sites) given in Figure 1. Transfer functions from the quarter-wavelength GRA are also shown in Figure 1 (these are referred to as theoretical transfer functions, TTFs). The input parameters for NRATTLE include shear wave velocity (V_S), soil density, and the intrinsic attenuation of shear-waves (Q_S^{-1}) which represents damping. Profiles of V_S are available from the KiK-net web site (*http://www.kyoshin.bosai.go.jp*). Soil density was estimated from P-wave velocity using the procedures suggested by Boore (2008), and Q_S^{-1} was estimated using a grid-search algorithm to optimize the fit to $H(f)$.

Figure 1(a) provides an example of poor fit between the ETF and TTF whereas Figure 1(b) shows a good fit. Goodness-of-fit was quantified using Pearson's sample correlation coefficient (r); a value of $r=0.6$ was taken by Thompson et al. as the threshold for good fit. The corresponding r values for the two sites in Figure 1 are 0.10 for the poor fit site and 0.79 for the good fit site. Dispersion curves (phase velocity vs. frequency) for the two example sites are shown in Figure 1. The results show that there is a large degree of variability in the dispersion curves for the poor-fit site and consistency in the dispersion curves for the good-fit site. These

and other similar results for additional sites indicate that geologic complexity, as reflected by spatial variability in the Rayleigh wave velocity structure, may correlate to the accuracy of GRA prediction. More complex geologic structure would be expected to produce 3D site effects that are not captured by GRA.
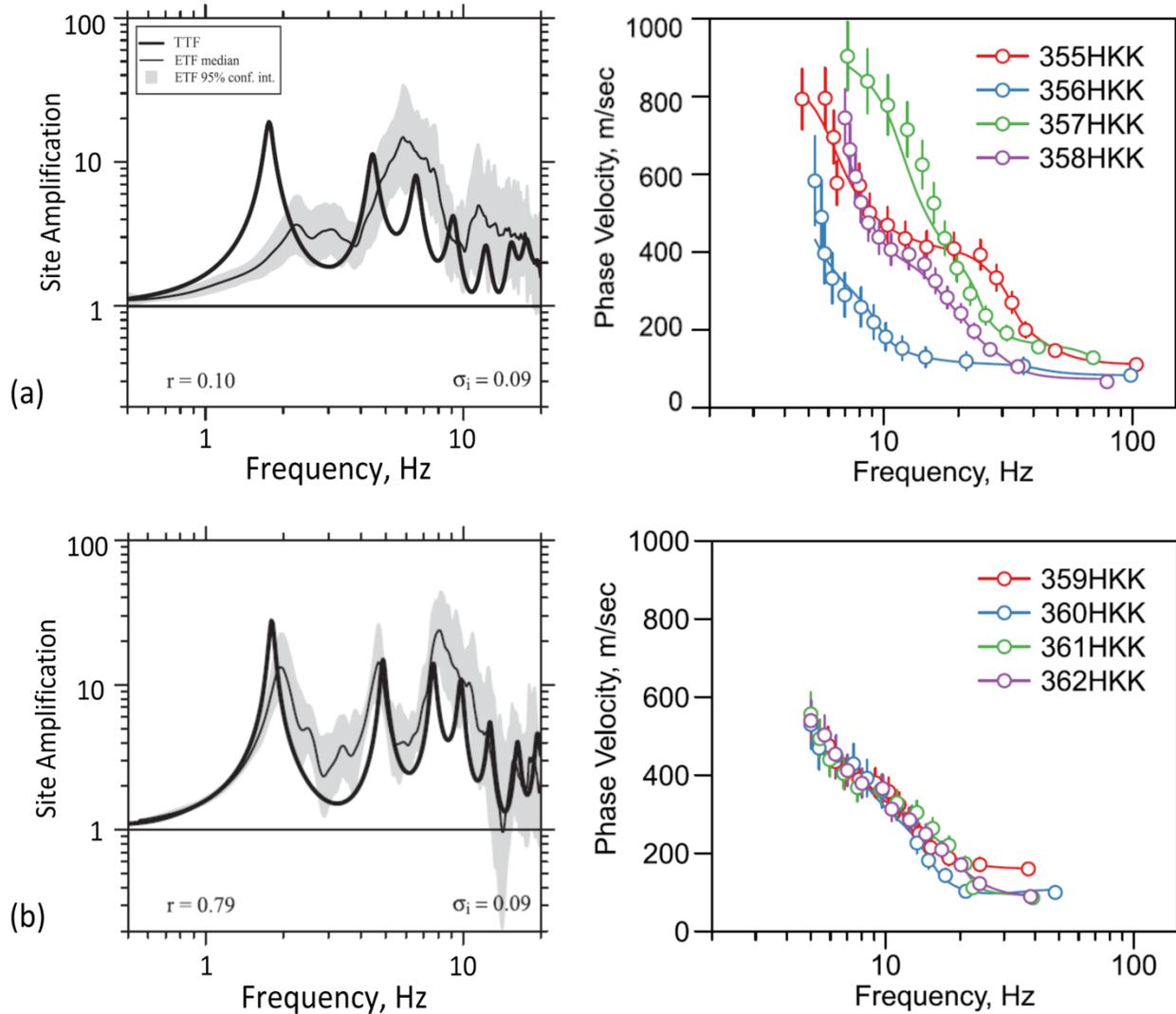

Figure 1. Examples of a poor fit (a) and good fit (b) between ETF and TTF at two KiK-net sites along with the dispersion curves from multiple SASW tests for both sites (adapted from Thompson et al., 2012)

Results for the 100 considered sites show that only 18% have a good fit between ETFs and TTFs, indicating 1D GRA fails to provide an accurate estimation of site response for a larger majority of KiK-net sites. Subsequent to Thompson et al. (2012), Kaklamanos et al. (2013) use subsets of KiK-net sites where a good ETF-TTF fit was obtained to study the issue identified in the introduction (i.e., when increased levels of sophistication in nonlinear modeling is needed in GRA). In this study, we do not screen sites to identify those for which the ETF matches the

shape of a TTF; instead we seek to understand how frequently such a match is achieved in relatively weak motion data from California vertical array sites.

Inventory of Vertical Arrays and Their Recordings in CA

We have collected site data for 39 vertical arrays in California as listed in Table 1. Our main source of site properties and ground motion data is the Center for Engineering Strong Motion Data (CESMD) website *(http://www.strongmotioncenter.org/)*. Velocity profile data is available for some of the sites, and ground motion time series can be downloaded through a search engine. In addition, CESMD maintains an FTP folder containing a database of weaker motions for all vertical array and surface-only sites. We have also considered four sites owned and maintained by the University of California at Santa Barbara (UCSB). The site information and recorded motions for these sites are available at *http://nees.ucsb.edu/*.

Interestingly, a major factor limiting the inventory of usable vertical array sites in California is the availability of V_S profile data; of the 39 vertical arrays, we have been able to collect usable V_S profile data for 30 sites (26 CESMD, 4 UCSB), and boring logs are available for 24 sites (22 CESMD and 2 UCSB). Given the relative cost of array installation (high) vs V_S profile development (low), a priority in future work should be to fill this data gap.

For our study, we utilize vertical array sites with measured V_S profile and having at least five pairs of surface/downhole recordings to increase the statistical significance of ETFs. The location of the vertical array sites are shown in Figure 2. The sites shown in blue were considered in the present work. .
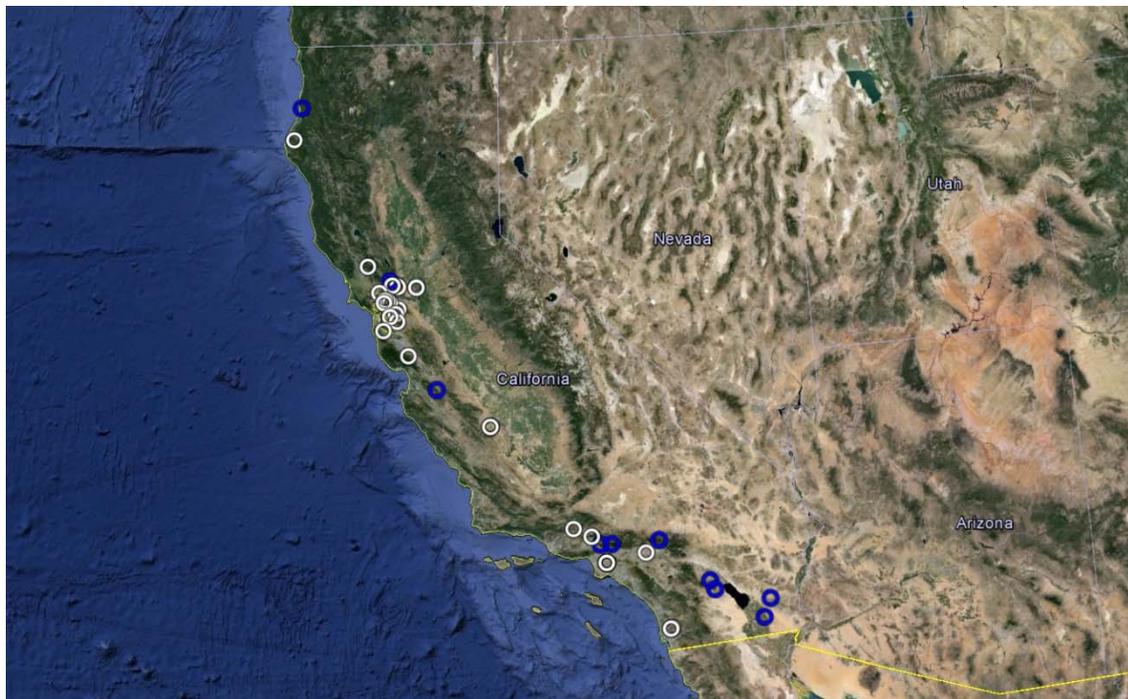

Figure 2. The location of vertical array sites in California (The sites used in this study are shown in blue)

Table 1. Summary of site characteristics for California vertical arrays. Sites considered in present work are bolded.

Station NO	Station Name	Owner	Low-amp. recs?[1]	# Rec	Latitude	Longitude	V_{S30} (m/s)	V_S profile Depth (m)[2]	Geotech log?[2]
58137	Alameda - Posey & Webster Geotech Array	CGS - CSMIP	NA	7	37.790	-122.277	208 (inferred)	N	Y
67265	Antioch – San Joaquin River N Geo. Array	CGS	NA	1	38.038	-121.752	Problematic	60[*]	N
67266	Antioch – San Joaquin River S Geo. Array	CGS	N	1	38.018	-121.752	272	105	Y
47750	Aptos - Seacliff Bluff Array	CGS - CSMIP	NA	4	36.972	-121.910	463	N[**]	N
68321	Benicia – Martinez Br N Geotech Array	CGS - CSMIP	N	3	38.051	-122.128	582	31	Y
68323	Benicia – Martinez Br S Geotech Array	CGS - CSMIP	N	4	38.033	-122.117	546	31	Y
13186	Corona – I15/Hwy 91 Geotech Array	CGS - CSMIP	N	2	33.882	-117.549	349	37	Y
68206	Crockett – Carquinez Br Geotech Array #1	CGS - CSMIP	N	4	38.054	-122.225	345	43	Y
68259	Crockett – Carquinez Br Geotech Array #2	CGS - CSMIP	N	4	38.055	-122.226	--	N	Y
1794	**El Centro – Meloland Geotechnical Array**	**CGS - CSMIP**	**Y**	**32**	32.774	-115.449	**182**	**240**	**Y**
89734	**Eureka - Geotechnical Array**	**CGS - CSMIP**	**Y**	**23**	40.819	-124.166	**194**	**225**	**Y**
58968	Foster City – San Mateo Br Geotech Array	CGS - CSMIP	N	1	37.573	-122.264	195	31	N
58964	Half Moon Bay - Tunitas Geotech Array	CGS - CSMIP	N	2	37.358	-122.398	309	39	Y
58487	Hayward - I580/238 West Geotech Array	CGS	N	1	37.689	-122.107	223	88	Y
58798	Hayward – San Mateo Br Geotech Array	CGS	N	1	37.617	-122.154	185	93	Y

Station NO	Station Name	Owner	Low-amp. recs?[1]	# Rec	Latitude	Longitude	V_{S30} (m/s)	V_S profile Depth (m) [2]	Geotech log? [2]
24703	**Los Angeles – La Cienega Geotech Array**	**CGS - CSMIP**	**Y**	**19**	34.036	-118.378	**241**	**280**	**Y**
24400	**Los Angeles - Obregon Park**	**CGS - CSMIP**	**Y**	**23**	34.037	-118.178	**449**	**64**	**Y**
14783	Los Angeles – Vincent Thm Geo Array W1	CGS - CSMIP	N	3	33.750	-118.275	149	192	N
14784	Los Angeles – Vincent Thm Geo Array W2	CGS - CSMIP	N	3	33.750	-118.278	149	195	N
14786	Los Angeles – Vincent Thos W Geo Array	CGS - CSMIP	N	1	33.750	-118.280	149	192	Y
24185	Moorpark - Hwy118/Arroyo Simi Geo. Array	CGS - CSMIP	NA	1	34.288	-118.865	--	N	Y
58204	Oakland – Bay Bridge Geotech Array	CGS - CSMIP	NA	3	37.821	-122.327	Problematic	155[*]	N
58526	Palo Alto – Dumbarton Br W Geotech Array	CGS	NA	1	37.499	-122.129	123	N[**]	Y
36529	Parkfield – Turkey Flat #1	CGS - CSMIP	N	3	35.878	-120.359	907	N[**]	N
36520	Parkfield – Turkey Flat #2	CGS - CSMIP	N	1	35.882	-120.351	467	N[**]	N
89289	Petrolia - Downhole [abandoned]	CGS - CSMIP	NA	1	40.317	-124.292	--	N	N
68797	Rohnert Park - Hwy 101 Geotech Array	CGS - CSMIP	N	2	38.347	-122.713	223	47.5	N
23792	**San Bernardino - I10/215 W Geotech Array**	**CGS - CSMIP**	**N**	**5**	34.064	-117.298	**271**	**92**	**Y**
3192	San Diego – Coronado East Geotech Array	CGS - CSMIP	N	2	32.698	-117.145	315	89	Y
3193	San Diego – Coronado West Geotech Array	CGS - CSMIP	N	2	32.688	-117.164	209	102	Y
58961	San Francisco – Bay Bridge Geotech Array	CGS - CSMIP	N	3	37.787	-122.389	387	36	Y

Station NO	Station Name	Owner	Low-amp. recs?[1]	# Rec	Latitude	Longitude	V_{S30} (m/s)	V_S profile Depth (m)[2]	Geotech log?[2]
58267	San Rafael – Richmond Brdg Geotech Array	CGS	N	1	37.943	-122.481	921	42	N
24764	Tarzana – Cedar Hill B	CGS - CSMIP	N	4	34.161	-118.535	302	N	N
58642	Treasure Island - Geotechnical Array	CGS - CSMIP	N	3	37.825	-122.374	159	120	N
68310	**Vallejo - Hwy 37/Napa River E Geo. Array**	**CGS - CSMIP**	**Y**	**17**	38.122	-122.275	**509**	**42**	**Y**
UCSB Arrays	**Garner Valley Downhole Array**	**UCSB**	--	**20**	33.401	-116.403	**240**	**210**	**Y**
UCSB Arrays	**Wildlife Liquefaction Array**	**UCSB**	--	**45**	33.058	-115.318	**203**	**98**	**Y**
UCSB Arrays	**Borrego Valley Field Site**	**UCSB**	--	**21**	33.259	-116.321	**350**	**230**	**N**
UCSB Arrays	**Hollister Digital Array**	**UCSB**	--	**23**	36.453	-121.365	**359**	**185**	**N**

[1]NA: Not applicable; we have not sought low-amplitude recordings because site not useful due to lack of V_S profile.
    N: Data may be available but not yet obtained.
[2]Y: Data available; N: Data not available.
[*] Top 20m is missing in the V_S measurements.
[**] There is V_S measurements, but not available at CESMD website.

Data Selection and Processing

Unprocessed records for the sites identified in the previous section were downloaded from CESMD and the nees.ucsb websites. Acceleration time series were visually inspected to identify and exclude low-quality, noise-dominated records. The data were processed using procedures developed in the NGA-West2 research project (Ancheta et al., 2014) and coded into an R routine (T. Kishida, *personal communication*, 2015). Low-cut and high-cut corner frequencies have been identified for each record by visual inspection, and low- and high-pass acausal Butterworth filters are used for filtering high and low frequency noise in the frequency domain. Baseline correction is also applied as needed.

Figure 3 shows an example of a record processed using these procedures, including time series (acceleration, velocity, displacement for processed record) and Fourier amplitude spectra and pseudo-acceleration response spectra at 5% damping for the unprocessed and processed versions of the record. Based on the records we have been able to access and process thus far, the usable database currently includes 10 sites and 225 record pairs. Figure 4 shows the number of usable recor

ds as a function of period; the decrease as period increases is due to application of low-cut corner frequencies in the record processing. The longest usable period is taken as $(0.877/f_c)$, where f_c is the low-cut corner frequency selected in record processing.
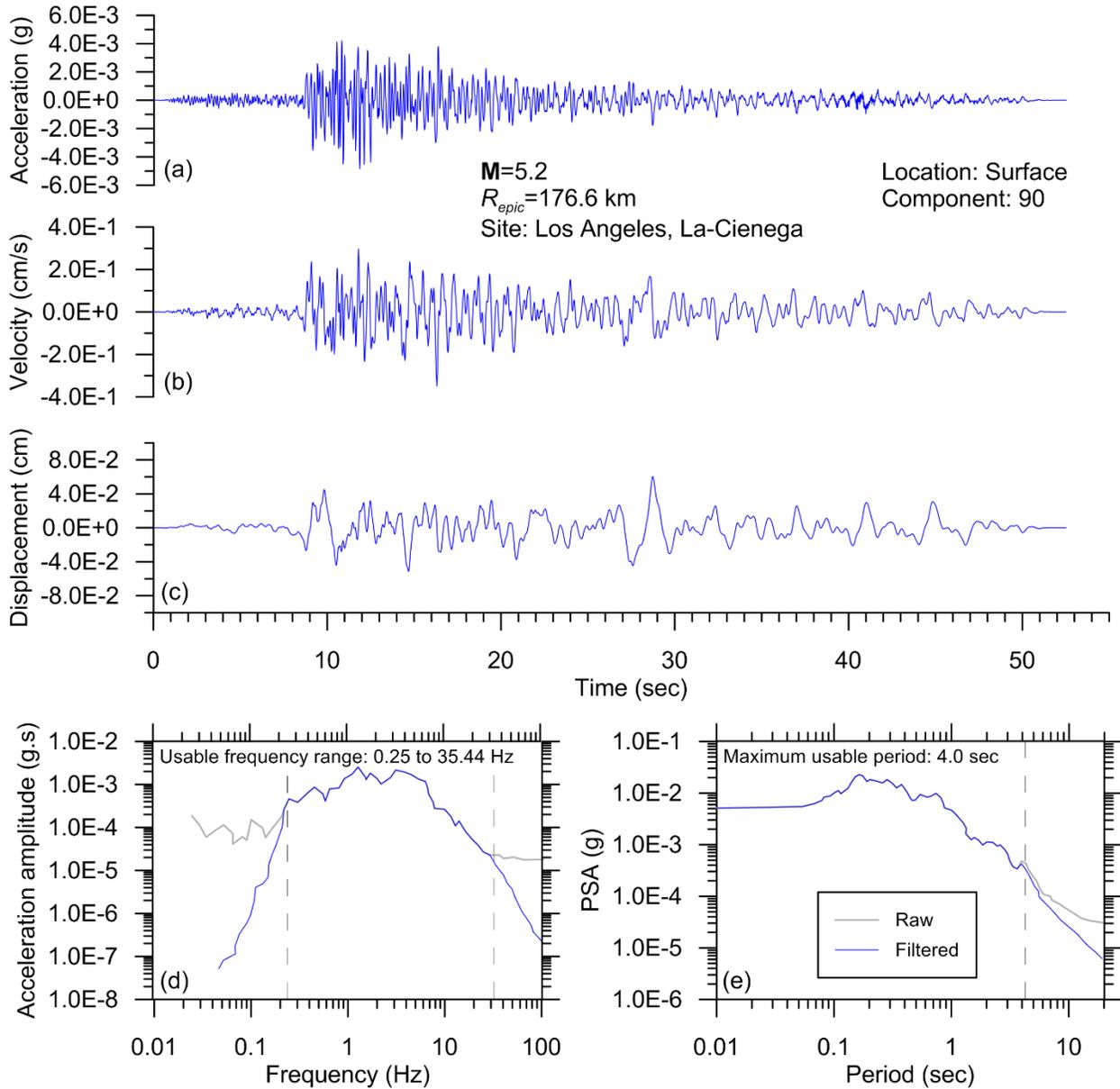

Figure 3. Example of record processed using PEER protocols developed in NGA-West2 project (Ancheta et al., 2014), including (a) acceleration time series, (b) velocity time series, (c) displacement time series, as well as (d) Fourier amplitude spectra and (e) pseudo-acceleration response spectra (PSA) at 5% damping for raw and filtered records.
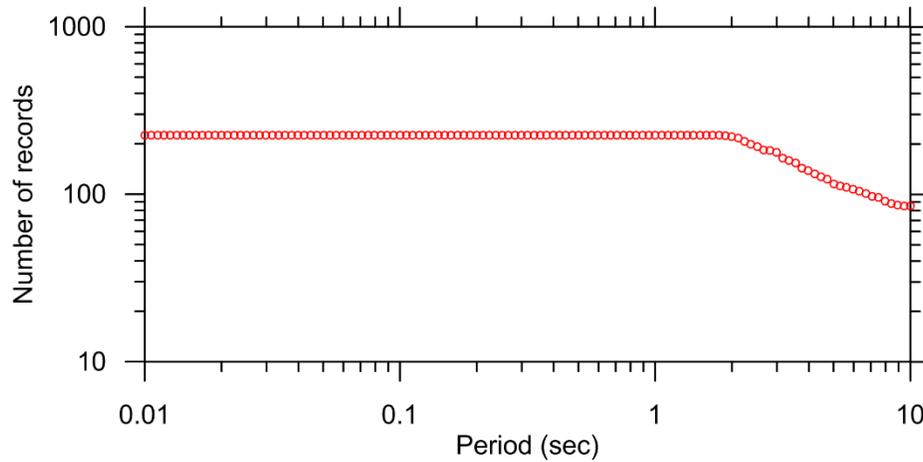
Figure 4. Number of available record pairs in the database according to their longest usable periods.

Analysis of Empirical Transfer Functions

Empirical transfer functions (ETFs) representing site response between the downhole and surface accelerometers are computed from ratios of Fourier amplitudes as given in Eq. (1). ETFs are only used over the usable frequency range based on record processing. The ETF is taken as the geometric-mean of ETFs for the two horizontal components of the recordings (at their as-recorded azimuths) for each site. The results shown subsequently are smoothed through the use of a Tukey (moving cosine) window with a width of 33 frequency steps (window width of approximately 0.5 Hz) in the frequency domain. This window size was selected for approximate compatibility with the prior work of Thompson et al. (2012).

We assume a log-normal distribution for ETF ordinates and compute for each site the median (μ_{ln}) (equivalent to the exponent of the natural log mean) and the natural log standard deviation of ETF (σ_{ln}) at each frequency using all available record pairs. Figure 5 shows example ETFs for all record pairs at the San Bernardino and Obregon Park sites along with the median and 95% confidence intervals of ETF. For plotting purposes, we show results over a frequency range between 0.5 and 10 Hz, which encompasses the usable frequency range for all records and focuses attention on frequencies that significantly contribute to PSA ordinates.
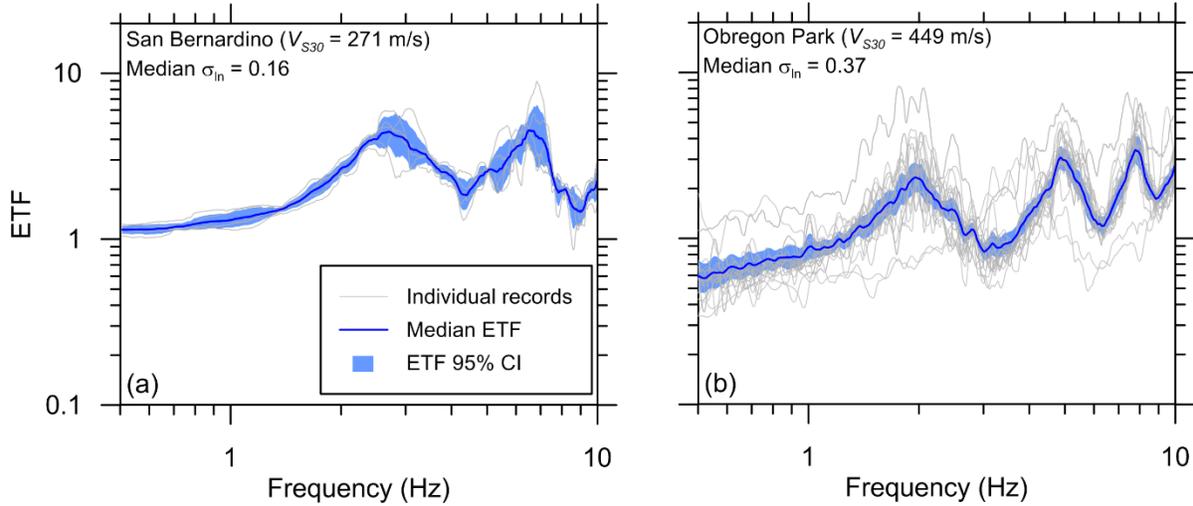
Figure 5. Empirical transfer functions plots for (a) San Bernardino site with low ETF variability, and (b) Obregon park with high ETF variability.

The two sites in Figure 5 have relatively low and high site response variability, as represented by frequency-dependent standard deviation term σ_{ln}. In order to represent this variability with a single metric that can be compiled for each site, we take the median σ_{ln} across the 0.5-10 Hz frequency range. These values are provided in Figure 5, being 0.11 for the low-variability site and 0.32 for the high-variability site.

Analysis of Theoretical Transfer Functions

Theoretical transfer functions (TTF) are computed by visco-elastic 1D GRA in DEEPSOIL. We exclude recordings with strong ground shaking (PGA at surface instrument > 0.1 g) so as to minimize nonlinear effects. Figure 6 shows histograms of PGA and PGV for the downhole instrument records used in the present work. We acknowledge that there are some records for which improved results could be obtained with EL procedures but have not undertaken such analyses to date with this data set.
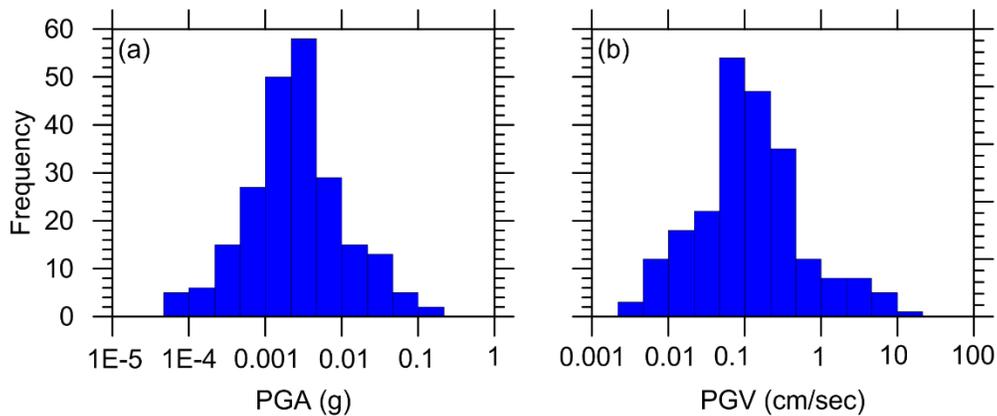

Figure 6. Histograms of PGA (a) and PGV (b) for downhole recordings used in this study.

Input soil properties for the visco-elastic analysis include the V_S profile, layer mass densities (assumed based on soil types and material descriptions), and material damping. Unlike Thompson et al. (2012), we utilize alternate approaches for estimating small-strain soil damping instead of back-calculating this parameter to optimize the ETF-TTF fit. These steps of considering alternate damping models are undertaken because best practices for selection of small-strain damping (D_{min}) are not well established (Stewart et al., 2014). Alternate approaches for modeling small-strain soil damping are described in the next section, which is followed by example results.

Damping Models

Laboratory-Based Models. We apply the traditional approach of taking damping from geotechnical laboratory cyclic testing, whereby the damping at small strains is taken as D_{min}^L. We estimate laboratory-based D_{min}^L using Darendeli (2001) relations for clays and silts, and Menq (2003) relations for granular soils. The input parameters for the D_{min}^L models are plasticity index (PI), overconsolidation ratio (OCR), and effective stress for Darendeli (2001), and mean grain size (D_{50}), coefficient of uniformity (C_u), and effective stress for Menq (2003). The D_{min}^L relations can only be used when geotechnical log and/or description of soil conditions are available for the site.

Depth-Dependent Q Factors. The effective material quality factor (Q_{ef}) can be estimated based on shear wave velocity using an empirical model developed by Campbell (2009) as follows:

$$Q_{ef} = 7.17 + 0.0276 V_S \tag{2}$$

Eq. (2) was derived by Campbell (2009) so as to match target site attenuation parameter (κ_0) for a sediment column in Memphis Tennessee. The value of Q_{ef} from Eq. (2) can be readily converted to soil damping as follows:

$$D_{min}(\%) = \frac{100}{2Q_{ef}} \tag{3}$$

This approach for modeling D_{min} does not require a geotechnical log.

Damping Estimated from κ_0 Model. Anderson and Hough (1984) showed that the shape of the Fourier amplitude spectrum for ground acceleration at high frequencies can be described as:

$$A(f) = A_0 \exp(-\pi \kappa f) \tag{4}$$

where κ is the controlling spectral decay parameter. Adopting the Hough and Anderson (1988) relationships and using notation from Campbell (2009), site attenuation parameter (κ_0) can be computed as:

$$\kappa_0 = \kappa_0^{rock} + \int_0^z Q_{ef}(z)^{-1} V_S(z)^{-1} dz \tag{5}$$

where κ_0^{rock} is the attenuation parameter for the bedrock, which sometimes matches the site condition at the downhole sensor. Using Eq. (3) to convert Q_{ef} to D, we re-write Eq. (5) as:

$$\kappa_0 = \kappa_0^{rock} + \int_0^z \frac{2D_{min}(z)}{100} V_S(z)^{-1} dz \qquad (6)$$

We take $\kappa_0^{rock} = 0.007$ sec as the mean estimate for western North America (Campbell, 2009), which then allows iterative adjustment of the D_{min} profile to match a target κ_0 value. The target κ_0 value is taken from an empirical global model conditional on V_{S30} (Van Houtte et al., 2011):

$$\ln(\kappa_0) = 3.490 - 1.062 \ln(V_{S30}) \qquad (7)$$

for which the standard error is 0.505 for the intercept and 0.076 for the slope.

We begin with the laboratory-based estimate of the D_{min} profile (D_{min}^L) and add a value (ΔD_i) at layer i. Modifying Eq. (6), we have:

$$\kappa_0 = \kappa_0^{rock} + \int_0^z \frac{2\left(D_{min}^L(z) + \Delta D_i\right)}{100} V_S(z)^{-1} dz \qquad (8)$$

We use three approaches for considering the depth-variation of ΔD_i: depth-invariant, depth-dependent per a prescribed relation, and V_S-dependent ΔD:

1- Depth-invariant $\Delta D_i = \Delta D_0$:

$$\Delta D_i = \Delta D_0 \qquad (9)$$

2- Visual inspection of D_{min}^L profiles at the subject sites, suggest that the following relation approximately captures typical trends for the soil conditions present at the sites:

$$D_{min}^L(z) = D_{min}^L(z=0)(z_i)^{-0.04} \qquad (10)$$

where z is the depth of the center of the layer in meters. This relation gives more weight to shallower layers. We propose a model for ΔD_i that follows this same trend:

$$\Delta D_i = \Delta D_0(z_i)^{-0.04} \qquad (11)$$

3- The V_S-dependent model is motivated by the negative correlation that exists between D_{min}^L and V_S at most sites. Based on visual inspection and some trial and error, we apply the following relation:

$$\Delta D_i = \Delta D_0 \left(\frac{V_S}{200}\right)^{-0.3} \qquad (12)$$

where V_S is the shear wave velocity for the layer in meters per second.

Eqs (9), (11), and (12) allow for single parameters (ΔD_0) to produce ΔD_i profiles, which can be used with Eq. (8) to compute κ_0. In our case, we take κ_0 from Van Houtte et al. (2011) and use Eq. (8) to compute three values of ΔD_0 for each site. For sites without a geotechnical log we do not have the D_{min}^L profile – in these cases we assume $D_{min}^L = 0$ for use with the above procedures.

Example Application

We apply the procedures described in the previous subsection for the El Centro-Meloland vertical array site. Figure 7 shows the geotechnical log, V_S profile, and damping profiles derived from the three approaches presented in the previous section. A considerable difference between damping profiles from the three approaches is evident, with the lab-based damping being smallest, the damping derived from κ_0 being largest, and the Campbell (2009) relation providing intermediate values. The alternate methods for capturing the depth-dependence of ΔD_i are seen to be of second-order importance as compared to the variations from the three modeling approaches for damping.
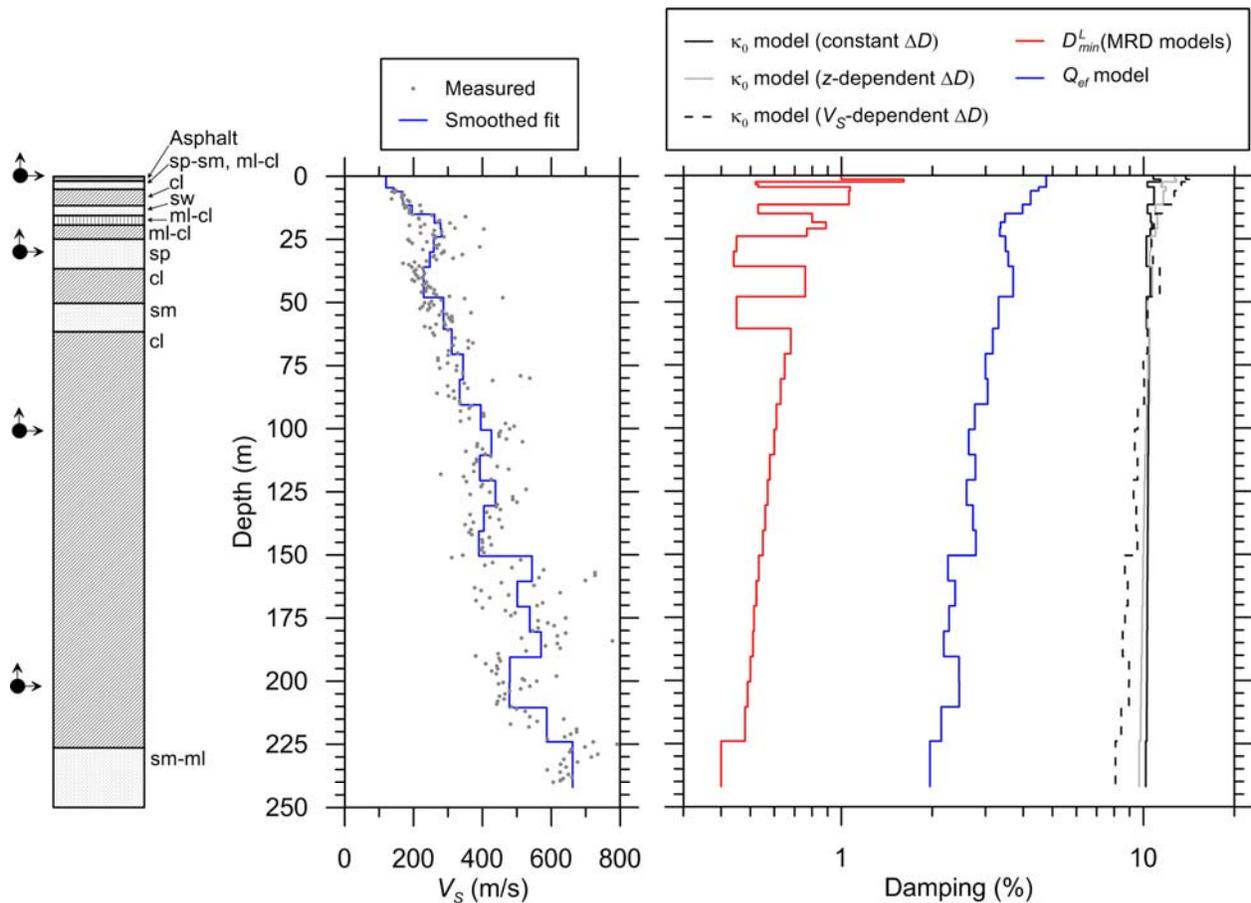
Figure 7. Site characteristics for El Centro-Meloland site including simplified geotechnical log, V_S profile, and soil damping profile estimated using empirical lab-based damping models by Darendeli (2001) and Menq (2003), damping derived from Q_{ef} model by Campbell (2009), and damping derived from κ_0 model by Van Houtte et al. (2011) (three alternate depth relations for ΔD).

Using the V_S profile, damping profiles (five alternatives), and estimated soil densities, we perform visco-elastic GRA in DEEPSOIL, and compute surface-downhole theoretical transfer functions (TTFs). As the downhole sensor is recording both up-going and down-going waves, we

take the boundary condition at the base of the model as rigid (Kwok et al., 2007). The visco-elastic analysis is performed in the frequency domain, and the site amplification predicted by the model is independent of the input motion. The resulting TTF is shown in Figure 8 for the El Centro-Meloland site. No smoothing was applied to these TTFs.

The overall shape and the position of the peaks in TTF plots (corresponding to modal frequencies of the site) are controlled by the V_S profile, and hence do not vary across damping models. However, the level of amplification at high frequencies is sensitive to damping levels, being much higher for low-damping approaches (lab-based) as opposed to high-damping approaches (κ_0-based).
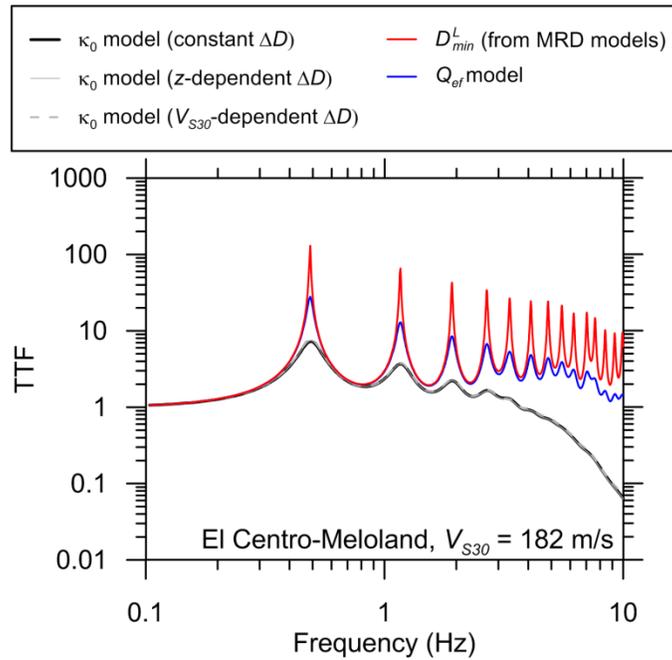

Figure 8. Plots of TTF vs. frequency using different approaches for estimating damping. El Centro-Meloland site

Model-Data Comparisons and Interpretation

Model-data comparisons can be visual by plotting together TTFs and ETFs. However, it is also useful to evaluate the goodness of fit, which we quantify with Pearson's sample correlation coefficient r (also used by Thompson et al., 2012) and the mean residual of the transfer function ($\bar{R}$). We define both metrics here and show example results.

Pearson's sample correlation coefficient (r)

We use this parameter as a measure of how well the model predictions and the data are correlated. Parameter r quantifies how well the shapes of the transfer functions align, including the locations and shapes of peaks. Parameter r is insensitive to relative overall levels of amplification, which is quantified in the next subsection. We calculate the Pearson's sample

correlation coefficient for i^{th} earthquake and j_{th} analysis (based on damping estimation approach) as follows for a given site:

$$r_{ij} = \frac{\sum \left(\text{ETF}_i(f) - \overline{\text{ETF}_i}\right)\left(\text{TTF}_j(f) - \overline{\text{TTF}_j}\right)}{\sqrt{\sum \left(\text{ETF}_i(f) - \overline{\text{ETF}_i}\right)^2} \sqrt{\sum \left(\text{TTF}_j(f) - \overline{\text{TTF}_j}\right)^2}} \tag{14}$$

where we take the summations between $f_{min} = 0.1$ and $f_{max} = 10$ Hz. The summation is performed over all frequency points between f_{min} and f_{max}. The average value of r across all events (r_j) for a given site is denoted $\overline{r}$.

Mean Transfer Function residual ($\overline{R}$)

We quantify bias in the prediction of site response transfer functions by computing the mean residual of predictions over all frequency points between f_{min} and f_{max}. The residuals are calculated for the ith earthquake and j^{th} damping estimation approach as follows:

$$R_{ij}(f) = \ln\left(\text{ETF}_i(f)\right) - \ln\left(\text{TTF}_j(f)\right) \tag{15}$$

where R_{ij} is the prediction residual. We average R_{ij} over all events and frequency points to calculate the overall bias for a site, which is denoted by $\overline{R}_j$. For sites with reasonably high values of $\overline{r}$, bias $\overline{R}_j$ provides an indication of how well alternate damping models fit the data.

Results and Interpretation

Figure 9 shows model-data comparisons for two example sites in which the fit is reasonably good (El Centro-Meloland) and relatively poor (San Bernardino). Figure 9 plots median for ETFs as well as TTFs based on the three principle soil damping models (we only show results for the second of the three κ_0-based approaches, given a lack of sensitivity). The TTFs in Figure 9 are smoothed in an equivalent manner to the ETFs.

For the El Centro-Meloland site (Fig 9a), the higher value of $\overline{r} = 0.30$ indicates relatively good alignment between the shapes of the ETF and TTF (the summary statistics shown in Fig. 9 apply for the Campbell 2009 damping formulation). In contrast, the San Bernardino site has a shape misfit between ETF and TTF and $\overline{r} = 0.06$. The general level of site amplification at high frequencies is better matched using the Campbell (2009) damping model than the other two models considered (the D_{min}^L model under-damps, the κ_0-based model over-damps). This result most often holds for other sites as well.

Based on preliminary results obtained thus far, California $\overline{r}$ values are higher, and median σ_{ln} values are lower, than their counterparts for the KiK-net arrays in Japan. This suggests that the ability of GRAs to match observation is better for the California vertical arrays than for KiK-net sites. This likely results from California sites mostly being located within large sedimentary basins, whereas KiK-net sites are often on firmer ground conditions (often weathered rock or thin soil over rock). The California sites with poor matches of data to model,

including the San Bernardino array, tend to be located near basin edges, where heterogeneous velocity structure is relatively likely to be present.
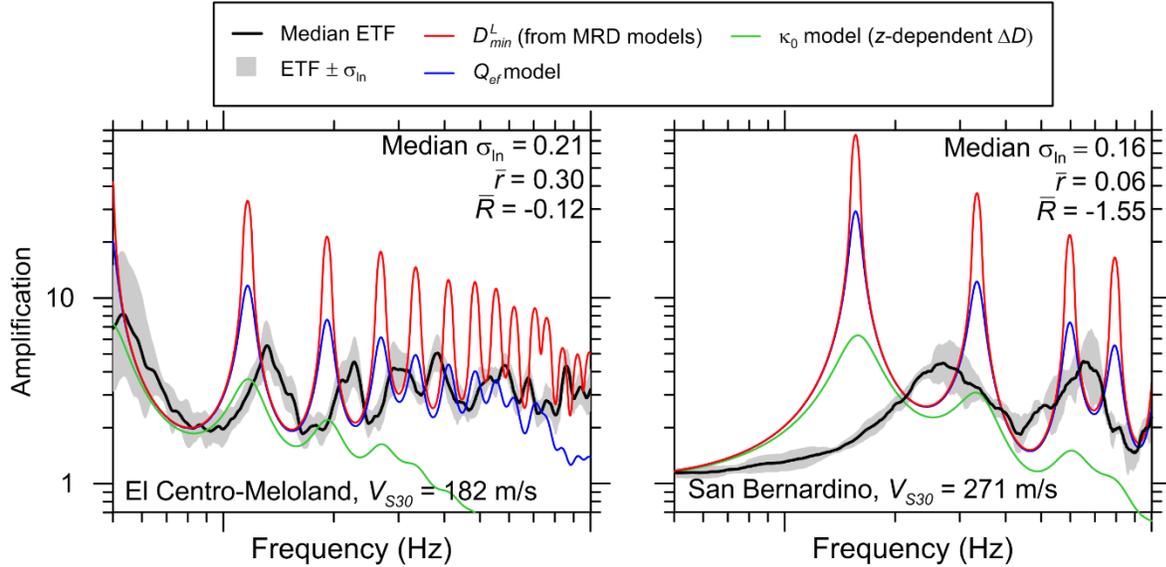

Figure 9. Comparison of ETF and TTFs for sites with good (El Centro-Meloland) and poor (San Bernardino) matches. Indicated values of $\bar{r}$ and $\bar{R}$ are based on Campbell (2009) damping model.

Conclusions

The motivation for this work is to examine whether the very low rate of match between 1-D ground response analysis (1D GRA) results and vertical array data observed in prior research in Japan (KiK-net array) is also found in vertical array data from California. We have compiled basic information for 39 vertical array sites in California; however, to date we have been able to use only 10 of these sites. In some cases, sites are not usable because of lack of measured V_S profiles. We compute theoretical transfer functions by performing 1D GRA using a visco-elastic procedure with three different damping models. We compute empirical transfer functions from the recordings that are generally of sufficiently low amplitude that the site response can be considered to be approximately linear. Pearson's sample correlation coefficients ($\bar{r}$) are used to quantify the alignment of transfer function shapes and mean residuals ($\bar{R}$) are used to quantify average data-model bias.

Our results show that a V_S-based damping model derived for sites in the eastern US (Campbell 2009) provides a better match of GRA results to data than damping evaluated from laboratory tests or damping derived to be compatible with relationships with spectral attenuation parameter κ_0. We find that a higher percentage of California sites, as compared to KiK-net sites, have a reasonably good match of empirical and theoretical transfer functions, as demonstrated by higher (on average) $\bar{r}$ values. The empirical transfer functions also have a greater degree of event-to-event consistency, as reflected by lower (on average) standard deviations of empirical transfer function ordinates. While these results are encouraging, it is notable that cases with a poor match also occur at some of the California sites investigated here, suggesting that 1D GRA

does not provide a suitable means by which to estimate site response for those sites. Understanding on an *a priori* basis, when GRA is unlikely to be effective remains an unsolved problem and an important priority for future research.

Acknowledgments

References

Anderson, J.G., and Hough, S.E. (1984). A model for the shape of the Fourier amplitude spectrum of acceleration at high frequencies, *Bull. Seismol. Soc. Am*. 74, 1969-1993.

Aoi, S. ,Obara, K., Hori, S., Kasahara, K., Okada, Y. (2000). New Japanese uphole–downhole strong-motion observation network: KiK-Net, Seismological Research Letters *Seism. Res. Lett.* 72:239.

Ancheta, T.D., Darragh, R.B., Stewart, J.P., Seyhan, E., Silva, W.J., Chiou, B.S.-J., Wooddell, K.E., Kottke, A.R., Boore, D.M., Kishida, T., and Donahue, J.L. (2014). NGA-West2 database, *Earthquake Spectra* 30, 989–1005.

Boore, D.M. (2005). SMSIM-Fortran programs for simulating ground motions from earthquakes: version 2.3. A revision of U.S. Geological Survey Open-File Report 96-80-A:55.

Boore, D.M. (2008). Some thoughts on relating density to velocity <http://quake.wr.usgs.gov/boore/daves_notes/daves_notes_on_relating_density_to_velocity_v1.2.pdf>

Campbell, K.W. (2009). Estimates of shear-wave Q and κ_0 for unconsolidated and semiconsolidated sediments in Eastern North America, *Bull. Seismol. Soc. Am*. 99, 2365-2392.

Darendeli M.B. (2001). Development of a New Family of Normalized modulus reduction and material damping curves, PhD Thesis, Department of Civil Engineering, University of Texas, Austin, TX.

Hashash, Y.M.A (2015). DEEPSOIL Version 6.0 User Manual and Tutorial, University of Illinois at Urbana-Champaign, Urbana, IL.

Hough, S.E., and Anderson, J.G. (1988). High-frequency spectra observed at Anza, California: Implications of Q structure, *Bull. Seismol. Soc. Am*. 78, 692-707.

Kaklamanos, J., Baise, L.G., Thompson, E.M., Dorfmann, L. (2015). Comparison of 1D linear, equivalent-linear, and nonlinear site response models at six KiK-net validation sites, *Soil Dyn. Earthq. Eng.* 69, 207-215.

Kaklamanos, J., Bradley, B.A., Thompson, E.M., and Baise, L.G. (2013). Critical parameters affecting bias and variability in site-response analyses using KiK-net downhole array data, *Bull. Seismol. Soc. Am*. 103, 1733–1749.

Kim, B., and Hashash, Y.M.A. (2013). Site response analysis using downhole array recordings during the March 2011 Tohoku-Oki Earthquake and the effect of long-duration ground motions." *Earthquake Spectra* 29, S37–S54.

Kim, B., Hashash, Y.M.A., Stewart, J.P., Rathje, E.M., Harmon, J.A., Musgrove, M.I., Campbell, K.W, and Silva, W.J. (2015). Relative differences between nonlinear and equivalent-linear 1D site response analyses, submitted to *Earthquake Spectra*. In review.

Kwok, A.O.L., Stewart J.P., Hashash, Y.M.A., Matasovic, N., Pyke, R.M., Wang, Z.L., and Yang, Z. (2007). Use of exact solutions of wave propagation problems to guide implementation of nonlinear seismic ground response analysis procedures, *J. Geotech. Geoenvir. Eng*. 133, 1385-1398.

Menq F.Y. (2003). Dynamic Properties of Sandy and Gravelly Soils, PhD Thesis, Department of Civil Engineering, University of Texas, Austin, TX.

Mikami, M., Stewart, J.P., Kamiyama, M. (2008). Effects of time series analysis protocols on transfer functions calculated from earthquake accelerograms, *Soil Dyn. Earthquake Eng*. 28, 695-706.

Stewart, J.P., Afshari, K., and Hashash, Y.M.A. (2014). Guidelines for performing hazard-consistent one-dimensional ground response analysis for ground motion prediction, *PEER Report No. 2014/16*, Pacific Earthquake Engineering Research Center, UC Berkeley, CA.

Thompson, E.M., Baise, L.G., Tanaka, Y., and Kayen, R.E. (2012). A taxonomy of site response complexity, *Soil Dyn. Earthquake Eng*. 41, 32-43.

Van Houtte, C., Drouet, S., Cotton, F. (2011). Analysis of the origins of κ (kappa) to compute hard rock to rock adjustment factors for GMPEs, *Bull. Seismol. Soc. Am*. 101, 2926-2941.

Zalachoris, G., and Rathje E.M. (2015). Evaluation of one-dimensional site response techniques using borehole arrays, *J. Geotech. Geoenviron. Eng.*, 10.1061/(ASCE)GT.1943-5606.0001366, 04015053.